Water Research 109 (2017) 358–366

Contents lists available at ScienceDirect

Water Research

journal homepage: www.elsevier.com/locate/watres

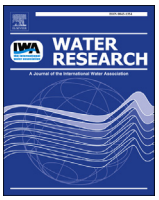

Roles of cation valance and exchange on the retention and colloid-facilitated transport of functionalized multi-walled carbon nanotubes in a natural soil

Miaoyue Zhang [a, d], Scott A. Bradford [b, *], Jirka Šimůnek [c], Harry Vereecken [a], Erwin Klumpp [a]

[a] Agrosphere Institute (IBG-3), Forschungszentrum Jülich GmbH, 52425 Jülich, Germany
[b] United States Department of Agriculture, Agricultural Research Service, U. S. Salinity Laboratory, Riverside, CA 92507, USA
[c] Department of Environmental Sciences, University of California Riverside, Riverside, CA 92521, USA
[d] Institute for Environmental Research (Biology V), RWTH Aachen University, Worringerweg 1, 52074 Aachen, Germany

ARTICLE INFO

Article history:
Received 18 August 2016
Received in revised form
28 November 2016
Accepted 28 November 2016
Available online 29 November 2016

Keywords:
Multi-walled carbon nanotubes
Soil
Breakthrough curves
Retention profiles
Cation exchange
Soil fractionation

ABSTRACT

Saturated soil column experiments were conducted to investigate the transport, retention, and release behavior of a low concentration (1 mg L^{-1}) of functionalized ^{14}C-labeled multi-walled carbon nanotubes (MWCNTs) in a natural soil under various solution chemistries. Breakthrough curves (BTCs) for MWCNTS exhibited greater amounts of retardation and retention with increasing solution ionic strength (IS) or in the presence of Ca^{2+} in comparison to K^{+}, and retention profiles (RPs) for MWCNTs were hyper-exponential in shape. These BTCs and RPs were well described using the advection-dispersion equation with a term for time- and depth-dependent retention. Fitted values of the retention rate coefficient and the maximum retained concentration of MWCNTs were higher with increasing IS and in the presence of Ca^{2+} in comparison to K^{+}. Significant amounts of MWCNT and soil colloid release was observed with a reduction of IS due to expansion of the electrical double layer, especially following cation exchange (when K^{+} displaced Ca^{2+}) that reduced the zeta potential of MWCNTs and the soil. Analysis of MWCNT concentrations in different soil size fractions revealed that >23.6% of the retained MWCNT mass was associated with water-dispersible colloids (WDCs), even though this fraction was only a minor portion of the total soil mass (2.38%). More MWCNTs were retained on the WDC fraction in the presence of Ca^{2+} than K^{+}. These findings indicated that some of the released MWCNTs by IS reduction and cation exchange were associated with the released clay fraction, and suggests the potential for facilitated transport of MWCNT by WDCs.

Published by Elsevier Ltd.

1. Introduction

Carbon nanotubes (CNTs) are allotropes of carbon with a cylindrical-shaped nanostructure (Iijima, 1991). They have been utilized in numerous commercial applications (Gohardani et al., 2014) such as electrical cables and wires (Janas et al., 2014), solar cells (Guldi et al., 2005), hydrogen storage (Jones and Bekkedahl, 1997), radar absorption (Lin et al., 2008) and considering as absorbents for environmental remediation and water treatment (Camilli et al., 2014; Li et al., 2012; Mauter and Elimelech, 2008; Pan and Xing, 2012; Zhang et al., 2010) due to their unique electric, chemical, and physical properties. The widespread commercial and potential environmental applications will undoubtedly result in their release into the subsurface. Current studies have investigated the transport behavior of CNTs in different porous media, which is affected by various physical and chemical conditions including ionic strength (IS), water content, grain size, input concentration and dissolved organic matter (Kasel et al., 2013a, 2013b; Tian et al., 2012; Yang et al., 2013). However, most of these studies were conducted in model soil systems such as rigorously cleaned sand or glass beads, which do not reflect the full complexity and heterogeneity of natural soils (e.g. complex grain size distribution and pore structure, and surface roughness and chemical heterogeneity)

* Corresponding author. United States Department of Agriculture, Agricultural Research Service, U. S. Salinity Laboratory, 450 W. Big Springs Road, Riverside, CA 92507, USA.
E-mail address: scott.bradford@ars.usda.gov (S.A. Bradford).

http://dx.doi.org/10.1016/j.watres.2016.11.062
0043-1354/Published by Elsevier Ltd.

(Cornelis et al., 2014). Kasel et al. (2013b) found limited transport of functionalized multi-walled carbon nanotubes (MWCNTs) in an undisturbed, natural soil. However, information on CNTs interactions with soil colloids and the potential for colloid-facilitated transport of CNT is still limited. Furthermore, the detachment or release of retained engineered nanoparticles (ENPs) like CNTs from the solid phase is important for predicting the ultimate fate and transport of ENPs in the subsurface, but has received little research attention.

Previous studies have demonstrated that pore-water chemistry plays an important role in controlling the retention of ENPs in soils (Badawy et al., 2010; Gao et al., 2006; Tian et al., 2012; Wang et al. 2014, 2015). Retention of ENPs is enhanced at higher ionic strength (IS) because the adhesive force increases with compression of the electric double layer (EDL) and a decrease in the magnitude of the surface potential (Elimelech et al., 2013; Israelachvili, 2011; Khilar and Fogler, 1998). Retention of ENPs is also higher in the presence of similar concentrations of divalent than monovalent cations (Torkzaban et al., 2012; Yang et al., 2013) because the double layer thickness and magnitude of the surface potential decreases and the IS increases to a greater extent (Elimelech et al., 2013; Israelachvili, 2011; Khilar and Fogler, 1998). In addition, adsorbed divalent cations, such as Ca^{2+}, can enhance retention of ENPs by creating nanoscale chemical heterogeneity on the solid surface that can neutralize or reverse the surface charge at specific locations (Grosberg et al., 2002) and/or produce a cation bridge between negatively charged sites on the surface of clays and ENPs (Torkzaban et al., 2012). The relative importance of solution IS and cation type on retention of ENPs is therefore expected to depend on the presence of soil colloids, but these complexities have not yet been fully resolved for natural soils.

A reduction in solution IS and cation exchange (monovalent displacing divalent cations) decreases the adhesive force and thereby induces release of clay particles and ENPs (Bradford and Kim, 2010; Grolimund and Borkovec, 2006; Liang et al., 2013; Torkzaban et al., 2013). The migration of soil colloids can facilitate the transport of pollutants and/or nanoparticles (Bradford and Torkzaban, 2008; Grolimund and Borkovec, 2005; Liang et al., 2013; Yan et al., 2016; Zhu et al., 2014). For example, Liang et al. (2013) provided experimental evidence that release of soil colloids with IS reduction and cation exchange can facilitate the transport of silver nanoparticles. Water-dispersible colloids (WDCs) are indicators for mobile soil colloids (de Jonge et al., 2004); e.g., WDCs are particles from the soil clay fraction that are less than 2 μm in size that are easily dispersible from soil with aqueous solution (Jiang et al., 2012, 2014). Knowledge of the interaction and association between ENPs and WDCs is therefore important for better understanding the fate of ENPs in soil. The effects of perturbations in solution chemistry on the release and colloid-facilitated transport of MWCNTs in soil have not yet been studied.

The objective of this study is to better understand roles of soil colloids, solution IS, and cation type on the transport, retention and release behavior of functionalized MWCNTs (1 mg L^{-1}) in a natural soil. Breakthrough curves and retention profiles for MWCNTs were determined in column experiments, and a numerical model was employed to simulate their fate. The retained concentration of MWCNTs was subsequently determined for the different soil size fractions (e.g., sand, silt, and WDCs). Other experiments were conducted to study the release of soil colloids and MWCNTs with perturbations in solution chemistry (e.g., IS reductions and cation exchange). Results provide valuable insight on the roles of cation type, chemical perturbations, and soil colloids on the retention, release and colloid-facilitated transport of MWCNTs. This knowledge can be useful for environmental applications and risk management of MWCNTs.

2. Materials and methods

2.1. Soil and MWCNT

Soil samples were collected from the upper 30 cm of an agricultural field site in Germany (Kaldenkirchen-Hülst, Germany), sieved to a fraction < 2 mm, and air dried. The soil was classified as a loamy sand with 4.9% clay (<2 μm), 26.7% silt (2–63 μm), and 68.5% sand (63–2000 μm). It had a median grain size (d_{50}) of 120 μm, a total organic carbon content of 1.1%, a cation exchange capacity of 7.8 $cmol_c\ kg^{-1}$, a pH value of 5.9 (0.01 M $CaCl_2$), a specific surface area of 1.7 $m^2\ g^{-1}$, and 0.8% iron. The clay faction was composed of illite, montmorillonite, and kaolinite minerals (Kasel et al., 2013b; Liang et al., 2013).

Radioactively (^{14}C) labeled and unlabeled functionalized MWCNTs (Bayer Technology Services GmbH, Leverkusen, Germany) were boiled with 70% nitric acid (Sigma-Aldrich Chemie GmbH, Steinheim, Germany) for 4 h to create additional oxygen-containing functional groups (e.g., carboxylic groups) on their surfaces (Kasel et al., 2013a). The functionalization and characterization of MWCNTs were previously described by Kasel et al. (2013a, 2013b). In brief, a transmission electron microscope was used to characterize morphological properties of MWCNTs, X-ray photoelectron spectroscopy was used to identify oxygen containing functional groups on MWCNTs, and inductively coupled plasma-mass spectrometry was used to determine the amount of metal catalysts before and after acid treatment of MWCNTs. The MWCNTs have a median diameter of 10–15 nm and a median length of 200–1000 nm (Pauluhn, 2010).

Suspensions of MWCNT at selected IS were prepared in deionized water with KCl and $CaCl_2$. These suspensions were dispersed by ultrasonicating the stock suspension for 15 min at 65 W, and then repeating this process 10 min before injection into soil columns. This low energy of sonication does not damage the MWCNTs (Li et al., 2012).

The hydrodynamic radius measured by dynamic light scattering (DLS) does not reflect the real geometric particle diameter for non-spherical particles like MWCNTs (Hassellöv et al., 2008; Pecora, 2000). Nevertheless, it can be used to study the aggregation behavior of functionalized MWCNTs suspensions. The hydrodynamic radius of unlabeled functionalized MWCNTs suspended in KCl and $CaCl_2$ at IS = 10 mM were measured 0, 1, and 4 h after suspension preparation by DLS using a Zetasizer Nano (Malvern ZetaSizer 4). The surface charge characteristics and electrophoretic mobility values of unlabeled functionalized MWCNT (pH ≈ 5.4) and crushed soil (pH ≈ 6) in selected electrolyte solutions were also determined using the Zetasizer Nano apparatus.

2.2. Transport and retention experiments

Saturated MWCNT transport experiments were conducted at different IS (1, 4, and 10 mM KCl) and different cation type at the same IS (1 mM KCl and $CaCl_2$, molar concentration 0.33 mM L^{-1} $CaCl_2$) by using stainless steel columns (3 cm inner diameter and 12 cm length) that were wet-packed with soil. Each side of the column was fitted with a stainless steel plate (1 mm opening) and double PTFE mesh (100 μm openings) to support the soil and to uniformly distribute the flow. The columns were wet packed by incrementally filling the column with soil and Milli-Q water, and then gently tapping the columns with a rubber mallet to ensure complete water saturation. Steady-state flow was achieved using a peristaltic pump, with the flow direction from the column bottom to the top. The saturated hydraulic conductivity and bulk density of the packed soil column was approximately 0.73 cm min^{-1} and 1.5 g cm^{-3}, respectively.

The soil in the column was equilibrated before initiating the transport experiment by injecting approximately 30 pore volumes (PVs) of a selected background electrolyte solution at a slow, constant Darcy velocity of 0.18 cm min^{-1}. Conservative tracer (KBr) and MWCNT transport experiments were then conducted sequentially at the same IS and cation type as the equilibrium phase, but at a higher, constant Darcy velocity of 0.71–0.73 cm min^{-1}. The conservative tracer experiment consisted of injecting a 2.1 PVs pulse (90 mL) of KBr solution, followed by continued eluting with the same bromide-free electrolyte solution for another 5.5 PVs. The effluent concentrations of bromide were determined using a high-performance liquid chromatograph (STH 585, Dionex, Sunnyvale, CA, USA) equipped with a UV detector (UV2075, Jasco, Essex, UK). Transport experiments for MWCNTs (input concentration, 1 mg L^{-1}) were conducted in a similar manner as the conservative tracer; e.g., injection of a 2.1 PVs pulse of MWCNT suspension, followed by elution with the same particle-free electrolyte solution for another 5.5 PVs. The ^{14}C-labeled effluent concentrations of MWCNT were determined using a liquid scintillation counter (LSC) (PerkinElmer, Rodgau, USA). After recovery of the breakthrough curve (BTC), the MWCNT retention profile (RP) was determined. Soil samples were excavated from a column in 0.5–1 cm increments, dried, crushed, combusted using a biological oxidizer at 900 °C (OX 500, R.J. Harvey Instrumentation Corporation, Tappan, NY, USA), and retained concentrations of MWCNTs in the soil were determined by LSC measurement. A summary of the experimental conditions is provided in Table 1.

2.3. Release experiments

Additional experiments were performed to study the release behavior of MWCNTs with IS reduction and cation exchange at a constant Darcy velocity of 0.71–0.73 cm min^{-1}. The initial deposition phase (step A) was conducted using MWCNTs (1 mg L^{-1}) in 10 mM KCl (experiment I), 1 mM $CaCl_2$ (experiment II), and 10 mM $CaCl_2$ (experiment III) solutions in an analogous fashion to MWCNTs transport experiments discussed above (Section 2.2). Release experiments II and III were then initiated by changing the eluting solution chemistry in the following sequence: Milli-Q water (step B); KCl at the same IS as in step A (step C); Milli-Q water (step D); 100 mM KCl (step E); and Milli-Q water (step F). Each solution chemistry step was conducted for 7.6 PVs. Experiment I consisted of only steps A and B. The ^{14}C-labeled effluent and soil concentrations of MWCNT were measured in the same manner as in transport experiments. Cation exchange and soil colloids were quantified during the release experiments by measuring the effluent concentrations of K, Ca, Fe, and Al by adding 5 mL of aqua regia for overnight digesting, diluting, and using inductively coupled optical emission spectrometry (ICP- OES). Because radioactive samples (^{14}C) are not allowed for ICP-OES measurement, the release experiments were repeated using unlabeled functionalized MWCNTs for this analysis. The effluent from the release experiment was also analyzed by DLS for soil colloids. A conservative tracer (KBr) experiment was repeated (Section 2.2) after a release experiment to assess potential changes in the hydrodynamic properties of the column.

2.4. Soil fractionation

Soil fractionation experiments were conducted to further elucidate the interactions between ^{14}C-labeled functionalized MWCNTs and the soil. The initial deposition phase was conducted similar to the MWCNT transport experiments discussed above (Section 2.2) at the same IS (1 mM KCl or $CaCl_2$). After recovery of the MWCNT breakthrough curve, all the soil was excavated from the column, dried, and then the soil particle-size was fractionated following the method of Séquaris and Lewandowski (2003). In brief, 100 g of dried soil was added to a 1 L Duran bottle (Schott, Mainz, Germany) containing 200 mL of the same electrolyte solution as the transport experiments (1 mM KCl or $CaCl_2$) and horizontally shaken at 150 rpm for 6 h. An additional 600 mL of the same electrolyte solution (1 mM KCl or $CaCl_2$) solution was then added to this bottle and mixed before sedimentation. The pipette method was then used to separate the soil into three size classes based on their sedimentation time according to Stoke's law (a particle density of 2.65 g cm^{-3} was assumed): (i) >20 μm (sand size) after 6 min; (ii) 2–20 μm (silt size) after 12 h; and (iii) <2 μm (water-dispersible colloids, WDCs) after 12 h. Triplicate 50 mL samples of the WDC suspension were further fractionated by centrifuging at 2525 × g for 4 min. Stoke's Law calculations indicated that the resulting supernatant consisted of electrolyte solution and the WDC fraction that was <0.45 μm, whereas the pellet was the WDC fraction that was 0.45–2 μm. Concentrations of MWCNTs that were associated with the sand, silt, 0.45–2 μm, and <0.45 μm fractions were determined by LSC in a similar manner to the transport experiments. Concentrations of MWCNTs in the column effluent and residual soil samples from columns that were not used for soil fractionation were measured to ensure mass balance. All the experiments were replicated and exhibited similar results.

2.5. Numerical modeling

The one-dimensional MWCNT transport was described by the HYDRUS-1D code (Šimůnek et al., 2016) using the advection-

Table 1
Experimental conditions, hydraulic parameters and mass balance information for all column experiments.

	IS [mM]	Co [mg L^{-1}]	q [cm min^{-1}]	Disp. [cm]	φ	M_{eff} [%]	M^*_{eff} [%]	M_{soil} [%]	M^*_{soil} [%]	M_{total} [%]	M^*_{total} [%]
Fig. 2	1, K^+	1	0.72	0.604	0.5	45.8	47.9	48.8	44.2	94.6	92.1
	4, K^+	1	0.72	0.364	0.51	13.8	11.7	77.2	85.9	91.0	97.6
	10, K^+	1	0.71	0.417	0.5	4	2.9	90.3	90.5	94.3	93.4
Fig. 3	1, K^+	1	0.72	0.604	0.5	45.8	47.9	48.8	44.2	94.6	92.1
	1, Ca^{2+}	1	0.72	0.711	0.5	4	3.6	91.8	93.2	95.8	96.8

	q [cm min^{-1}]	φ	IS_A [mM]	M_A [%]	M_B H_2O [%]	IS_C [mM]	M_C [%]	M_D H_2O [%]	IS_E [mM]	M_E [%]	M_F H_2O [%]	M_{soil} [%]	M_{total} [%]
Fig. 4	I, 0.71	0.47	10, K^+	4.6	42.2							45.1	91.9
	II, 0.72	0.49	1, Ca^{2+}	4.2	7.7	1, K^+	0.6	5.3	100, K^+	0.4	21.7	50.6	90.5
	III, 0.73	0.48	10, Ca^{2+}	0.03	0.3	10, K^+	0.02	11	100, K^+	0.6	11.6	64.8	88.4

Fig. 1: ionic strength effect; Fig. 2: cation type effect; Fig. 3: release of MWCNT by ionic strength reduction and cation exchange; Co, MWCNT input concentration; q, Darcy velocity; IS, ionic strength; φ,porosity; Disp.is the estimated longitudinal dispersivity; M_{eff}, M_{soil}, and M_{total} are mass percentages recovered from effluent, soil, and total, respectively; $M_A - M_F$ are the mass percentages recovered from effluent (Steps A–F) in release experiments.
M^*_{eff}, M^*_{soil}, M^*_{total} are mass percentages of the replicate experiments recovered from effluent, soil, and total, respectively. The data from the replicate experiments were not shown in Figs. 1 and 2.

dispersion equation with a kinetic retention site (Bradford et al., 2003; Kasel et al., 2013a, 2013b):

$$\theta\frac{\partial C}{\partial t}+\rho\frac{\partial S}{\partial t}=\theta D\frac{\partial^2 C}{\partial x^2}-q\frac{\partial C}{\partial x} \quad (1)$$

where θ is volumetric water content [L^3L^{-3}], ρ is the bulk density of the soil [ML^{-3}; where L and M denote units of length and mass, respectively], C is MWCNT concentration in the effluent [NL^{-3}; where N denotes number], t is the time [T; where T denotes units of time], x is the spatial coordinate [L], D is the hydrodynamic dispersion coefficient [L^2T^{-1}], q is the Darcy velocity [LT^{-1}], and S [NM^{-1}] is the solid phase concentrations of MWCNTs. The solid phase mass balance is given as:

$$\rho\frac{\partial S}{\partial t}=\theta\psi k_{sw}C-\rho k_{rs}S \quad (2)$$

where k_{sw} [T^{-1}] is the first-order retention rate coefficients, k_{rs} [T^{-1}] is the first-order release rate coefficients, and ψ [−] are dimensionless functions that account for time- and depth-dependent retention. The parameter ψ is equal to:

$$\psi=\left(1-\frac{S}{S_{max}}\right)\left(\frac{d_{50}+x}{d_{50}}\right)^{-\beta} \quad (3)$$

where S_{max} [NM^{-1}] is the maximum solid phase concentration, β [−] is a fitting parameter which controls the shape of the retention profile. The value of $\beta = 0.765$ was selected based on reported results for MWCNTs (Kasel et al., 2013a, 2013b).

HYDRUS-1D includes a provision to determine model parameters by inverse optimization to experimental data. Values of θ and the dispersivity (λ) were determined by fitting to the conservative tracer BTC, whereas retention model parameters (k_{sw}, k_{rs}, and S_{max}) were obtained by optimization to BTCs and RPs for MWCNTs.

3. Results and discussion

3.1. MWCNT suspension stability

The hydrodynamic radius of MWCNTs in KCl and $CaCl_2$ solutions at an IS = 10 mM was measured 0, 1, and 4 h after suspension preparation by DLS. The hydrodynamic radius was always within the measurement error, and did not show a systematic trend with the cation type or time. The MWCNT suspensions were therefore considered to be stable during the injection phase (approx. 18 min) of all transport and release experiments discussed below.

3.2. Zeta potential

Fig. 1 presents plots of measured zeta potentials (Fig. 1a) and electrophoretic mobility (Fig. 1b) values for MWCNTs and soil as a function of IS and cation valence (K^+ and Ca^{2+}). Both MWCNTs and soil exhibited a net negative charge for the considered solution chemistry conditions. This result indicates that net electrostatic interactions between the MWCNTs and soil were repulsive. The zeta potential was generally similar in magnitude for MWCNTs and soil under the same solution chemistry condition. Furthermore, increasing the solution IS and cation valence tended to decrease the magnitude of both zeta potentials. These trends are consistent with published literature (Elimelech et al., 2013; Liang et al., 2013; McNew and LeBoeuf, 2016).

3.3. Transport and retention of MWCNTs

Fig. 2 presents observed and simulated BTCs and RPs for functionalized MWCNTs when the IS = 1, 4, and 10 mM KCl. The BTCs (Fig. 2a) are plotted as the normalized effluent concentration (C/C_o; where C_o is the influent suspension concentration) versus pore volumes, whereas the RPs are plotted as normalized solid phase concentration (S/C_o) as a function of distance from the column inlet. The experimental conditions, hydraulic parameters (θ and λ), and mass balance information for these experiments are presented in Table 1. Simulations provided an excellent description of BTCs and RPs with a Pearson's correlation coefficient (R^2) > 0.95. Table 2 provides a summary of fitted retention model parameters.

The total mass balance (M_{total}) of column experiments in Fig. 2 was >91% (Table 1). The mass percentage recovered from the effluent (M_{eff}) strongly decreased from 45.8% to 4.0% as the IS increased from 1 to 10 mM (KCl), resulting in a corresponding increase in the solid phase mass percentage (M_{soil}) from 48.8% to 90.3%. Fitted values of k_{sw} and S_{max}/C_o also increased with IS, whereas k_{rs} decreased with IS. These trends are attributable to an increase in the adhesive force for MWCNTs on soil with IS due to compression of the double layer thickness and a decrease in the magnitude of the zeta potential (Fig. 1), and is consistent with other studies (Jaisi et al., 2008; Tian et al., 2012; Yang et al., 2013). It should also be mentioned that the influence of nanoscale heterogeneities on colloid retention increases with an increase in IS (Bradford and Torkzaban, 2013).

BTCs for MWCNTs (Fig. 2a) exhibited increasing breakthrough concentrations over time due to blocking; e.g., filling of a limited number of retention sites with continued MWCNT injection. The breakthrough time for MWCNTs was also delayed in comparison with the tracer (data not shown). This occurs because k_{sw} was sufficiently high to produce complete retention until available retention sites fill enough to induce breakthrough (e.g., Leij et al., 2015). This delay in breakthrough increases with IS because a larger value of S_{max}/C_o takes longer to fill. Other studies that have investigated the effect of IS on CNTs transport in clean sands or glass beads have not observed this result (Jaisi et al., 2008; Tian et al., 2012; Yang et al., 2013), but it has been previous demonstrated for other nanoparticles (e.g.,Sasidharan et al., 2014). This apparent discrepancy is due to the strong dependency of blocking on k_{sw}, S_{max}, C_o, and the input pulse duration (Leij et al., 2015). In particular, delay in the breakthrough will not occur if k_{sw}, C_o, and the input pulse duration is too low, or if S_{max} is too high.

The RPs for MWCNTs (Fig. 2b) exhibited a hyper-exponential shape that was well described using the model with a depth-dependent retention function (Eq. (3)). This indicates that a greater retention rate occurred near the column inlet then the outlet. Hyper-exponential RPs have previously been observed for MWCNTs (Kasel et al., 2013a, Kasel et al. 2013b). Liang et al. (2013) also observed hyper-exponential RPs for spherical silver nanoparticles (diameter of 15 nm) in this same soil. A variety of potential explanations for hyper-exponential RPs have been identified in the literature, including: straining (Bradford et al., 2002, 2003; Bradford and Bettahar, 2006), colloid aggregation (Chen and Elimelech, 2006, 2007), chemical heterogeneity on the soil and colloid (Tong and Johnson, 2007; Tufenkji and Elimelech, 2005), and system hydrodynamics (Bradford et al., 2009; Li et al., 2005). It is difficult to ascertain the potential contribution of each factor to the observed RP. However, MWCNTs retention still resulted in a hyper-exponential shape even under low IS conditions (1 mM KCl) that should minimize the contribution of colloid aggregation and chemical heterogeneity. Results for theoretical calculations that consider forces and torques that act on colloids near heterogeneous surfaces, and comparison of retention in batch and column studies

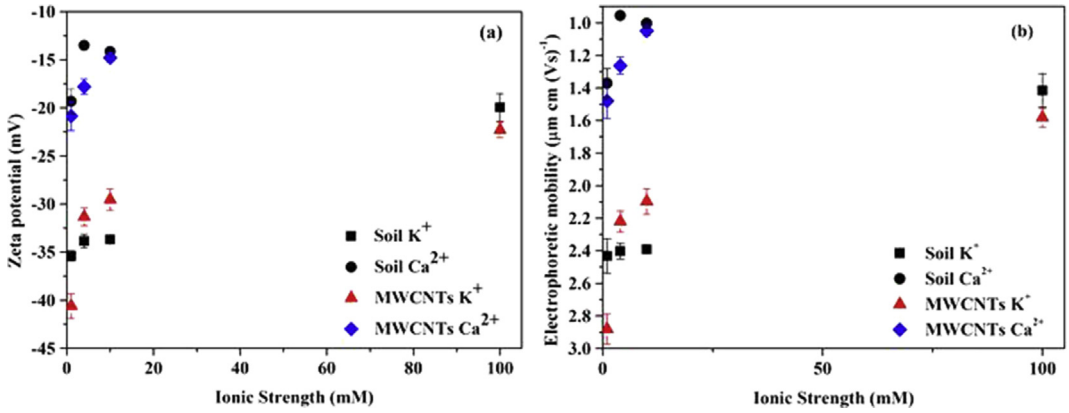

Fig. 1. Zeta potentials (a) and electrophoretic mobility (b) values of MWCNTs (pH ≈ 5.4) and soil (pH ≈ 6) as a function of the solution (KCl and $CaCl_2$) ionic strength.

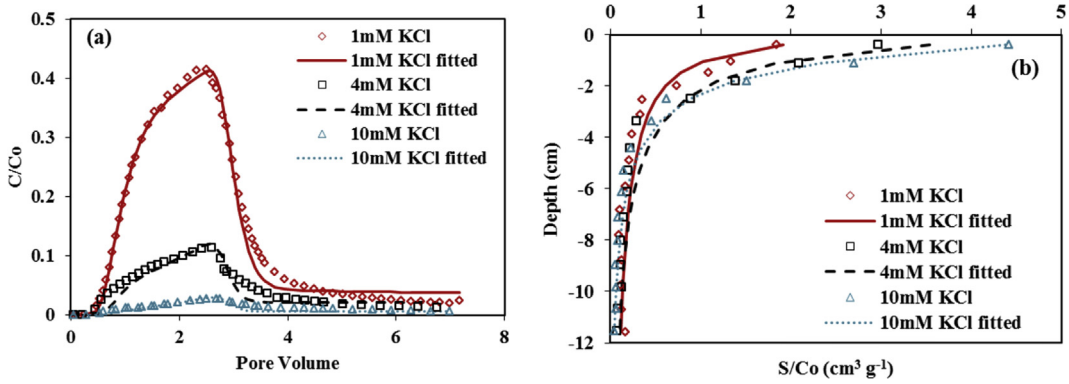

Fig. 2. Effect of ionic strength on the transport and retention of MWCNTs in soil: observed and fitted breakthrough curves (a) and retention profiles (b) of MWCNTs under 1, 4, and 10 mM KCl, respectively.

Table 2
Fitted model parameters.

	IS [mM]	β	S_{max}/C_o [$cm^3 g^{-1}$]	S.E. S_{max}/C_o	k_{sw} [min^{-1}]	S.E. k_{sw}	k_{rs} [min^{-1}]	S.E. k_{rs}	R^2
Fig. 2	1, K^+	0.765	5.45	1.51	10.30	5.89E-01	6.80E-03	5.00E-04	0.975
	4, K^+	0.765	5.98	NF	28.22	6.88E-01	5.70E-03	4.59E-04	0.958
	10, K^+	0.765	6.10	4.65E-01	49.69	1.17E+00	4.56E-03	1.30E-03	0.991
Fig. 3	1, K^+	0.765	5.45	1.51	10.30	5.89E-01	6.80E-03	5.00E-04	0.975
	1, Ca^{2+}	0.765	9.33	NF	44.54	1.39E+00	3.31E-03	1.34E-03	0.971

Fig. 1 ionic strength effect; Fig. 2: cation type effect; R^2 reflects the correlation of observed and fitted data; NF - denotes not fitted. k_{sw}, the first-order retention rate coefficient; k_{rs}, the first-order release rate coefficient; S_{max}/C_o, normalized maximum solid phase concentration of deposited MWCNTs; S.E. – standard error.

indicate that retention of MWCNTs is controlled by surface straining near macroscopic roughness locations and grain-grain contacts under low IS conditions (Bradford and Torkzaban, 2015; Zhang et al., 2016). Similarly, other studies have concluded that straining played a dominant role in the retention of MWCNTs (Jaisi et al., 2008; Kasel et al., 2013a, 2013b; Wang et al., 2012).

The effect of cation type on the transport and retention of MWCNTs in soil is presented in Fig. 3. In this case, MWCNTs were deposited and eluted at the same IS = 1 mM in the presence of monovalent K^+ or divalent Ca^{2+} cations. Fig. 3 presents observed and simulated BTCs and RPs. Table 2 summarizes the fitted retention model parameters that provided an excellent description of this data ($R^2 > 0.97$). Retention of MWCNTs (Table 1) and fitted values of k_{sw} and S_{max}/C_o (Table 2) were much higher in the presence of Ca^{2+} than K^+ at the same IS. In comparison to K^+, Ca^{2+} produces a stronger adhesive force due to the smaller magnitude of the zeta potential (Fig. 1), localized neutralization and/or reversal of surface charge (Grosberg et al., 2002), and cation bridging (Torkzaban et al., 2012) that all enhances retention of MWCNTs. Fitted values of S_{max}/C_o clearly indicate that many more retention sites were available in the presence of Ca^{2+} than K^+ (an increase of 171%). This large increase in the value of S_{max}/C_o in the presence Ca^{2+} also influenced the blocking behavior in the MWCNT BTC. In particular, a greater delay in the breakthrough time and a slower rate of increase in the BTC with time was observed (Fig. 3b). Similar to RPs in the presence of K^+ (Fig. 2b), the RP in the presence of Ca^{2+} also exhibited a hyper-exponential shape. This observation suggests that similar retention mechanisms were operative in the presence of both monovalent and divalent cations.

3.4. Release of MWCNTs

Very little release of MWCNTs was observed under steady-state solution chemistry conditions (Figs. 2 and 3, and Table 2). Conversely, significant amounts of colloid and nanoparticle release have been reported when transient solution chemistry reduce the

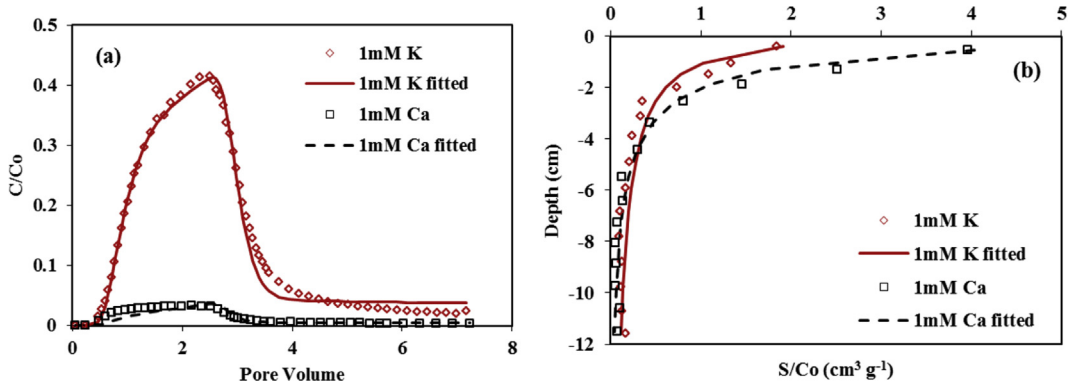

Fig. 3. Effect of cation type on the transport and retention of MWCNTs in soil: observed and fitted breakthrough curves (a) and retention profiles (b) of MWCNTs under 1 mM KCl and $CaCl_2$, respectively.

adhesive force (e.g., Liang et al., 2013). Additional experiments were therefore conducted to better understand the effect of IS reduction and cation exchange on the release of MWCNTs in soil. Step A of Fig. 4a presents BTCs when MWCNTs were retained and eluted in the presence of IS = 10 mM KCl (experiment I), and $CaCl_2$ solution at IS = 1 mM (experiment III) and IS = 10 mM (experiment III). Transport of MWCNTs was limited in Step A for all of these conditions. Indeed, effluent mass balance during step A (M_A) only equaled 4.6, 4.2, and 0.03% for experiments I, II, and III, respectively.

Step B in Fig. 4a presents the subsequent release curves when retained MWCNTS were eluted by Milli-Q water. Release was much more pronounced when the MWCNTs were retained (step A) in the presence of monovalent K^+ (42.2%) than divalent Ca^{2+} (<7.7%) cation. This result indicates that the adhesive interaction was stronger and less reversible in the presence of Ca^{2+} than K^+. Furthermore, release of MWCNTs was less pronounced when they were retained in IS = 10 mM $CaCl_2$ (0.3%) than IS = 1 mM $CaCl_2$ (7.7%) solution, respectively. This implies that a stronger adhesive force continued to act on the MWCNTs when they were initially retained in the presence of a higher concentration of Ca^{2+}. A potential explanation for these observations is due to localized charge neutralization/reversal or cation bridging by Ca^{2+} which creates strong interactions with MWCNTs (Jaisi et al., 2008; Liang et al., 2013).

Experiments II and III were continued to further study the release of MWCNTs that were retained in the presence of Ca^{2+} using the following elution sequence: KCl at the same IS as in step A (step C); Milli-Q water (step D); 100 mM KCl (step E); and Milli-Q water (step F). The effluent concentrations of MWCNTs during each of these steps are shown in Fig. 4a, with corresponding mass balance information given in Table 1 (denoted as M_C-M_F). Effluent concentrations of K^+ and Ca^{2+}, and Al and Fe in a replicate release experiment for MWCNT in IS = 1 mM $CaCl_2$ solution during step A are shown in Fig. 4b and c, respectively. The RPs for MWCNTs following completion of transient release experiments I, II, and III are shown in Fig. 4d.

MWCNT release always occurred when Milli-Q water was injected into the column during steps B, D, and F, but gradually ceased when KCl was injected during steps C and E (Fig. 4a). The amount of MWCNTs that was released with Milli-Q water strongly depended on the concentrations of injected Ca^{2+} during step A and K^+ during steps C and E. Release of MWCNTs that occurred with IS reduction during steps D and F were also influenced by the amount of cation exchange that occurred during steps C and E. Specifically, greater amounts of Ca^{2+} ions were exchanged back into the aqueous phase when a higher concentration of K^+ was injected (Fig. 4b). This exchange process reduced the strength of the adhesive interaction, such that greater amounts of MWCNTs were released with a subsequent reduction in solution IS. Consequently, M_D was less when the IS equaled 1 mM (M_D = 5.3%) than 10 mM (M_D = 11%) KCl during step C. The value of M_F was influenced by: (i) the initial concentration of Ca^{2+} during deposition (step A); (ii) the amount of cation exchange (steps C and E); and (iii) the previous amounts of MWCNT that were released (steps B and D). In this case, the value of M_F equaled 21.1 and 11.6% when the IS equaled 1 and 10 mM $CaCl_2$, respectively, during step A. A similar trend was observed for the total recovered mass of MWCNTs during steps A-F, and this indicates that increased strength of the adhesive force at a higher Ca^{2+} concentration (step A) was the dominant consideration.

Fig. 4d presents the RPs for MWCNTs following completion of the release experiments. Similar to Figs. 2 and 3, RPs were still hyper-exponential in shape. However, close inspection of Figs. 2b, 3b and 4d reveals that retained MWCNTs in release experiments were shifted from the top into deeper layers. This observation supports the potential for continued slow remobilization of MWCNTs in the subsurface due to the effects of IS reduction and cation exchange.

Bradford and Kim (2010) examined the release behavior of in situ kaolinite clay from sand due to cation exchange and IS reduction, and observed similar trends as seen for the MWCNTs in Fig. 4. This observation suggests the potential for colloid-facilitated transport of MWCNTs in this study. Indeed, effluent samples exhibited differences in sample turbidity due to release of soil colloids, and DLS measurements indicated the presence of soil colloids with hydrodynamic diameter ranged from 150 to 308 nm. To better understand the potential association of released MWCNTs and soil colloids, Fig. 4c presents plots of effluent concentrations of Al, Fe, and MWCNTs during the release experiment. Note that release behavior of Fe, Al, and MWCNTs closely follow each other with IS reduction and cation exchange. Liang et al. (2013) also observed this same phenomenon for silver nanoparticles with Al and Fe. All of these observations strongly support the potential for colloid-facilitated transport of MWCNTs during the release experiments. However, it should be mentioned that BTCs for the conservative tracer before and after release experiments were nearly identical (data not shown). This observation suggests that changes in the soil hydraulic properties due to soil colloid release were inconsequential during the release experiment.

3.5. Soil size fractionation

Soil fractionation was conducted following completion of MWCNT transport experiments at IS = 1 mM in KCl and $CaCl_2$

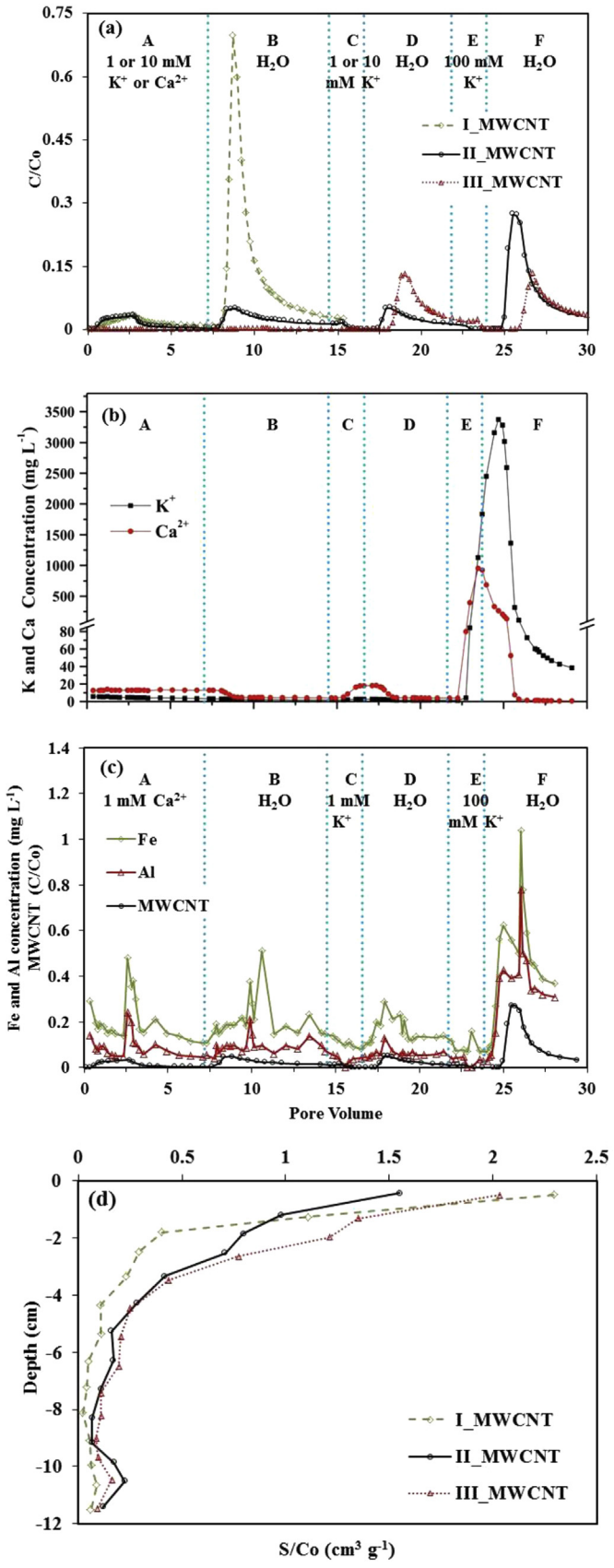

Fig. 4. (a) Breakthrough and release behavior, and retention profiles (d) of MWCNTs in soil. Deposition (step A) occurred at an IS = 10 mM using KCl for experiment I, and an IS = 1 and 10 mM using $CaCl_2$ for experiment II and III, respectively, whereas release was initiated by ionic strength reduction (steps B, D, and F, Milli-Q water) and cation exchange (steps C and E) as summarized in Table 1. (b) Effluent concentrations of K and Ca during steps A–F in experiment II. (c) Release of MWCNTs and naturally occurring minerals due to ionic strength reduction (steps B, D, and F, Milli-Q water) and cation exchange (steps C and E) in soil in experiment II. For experiment III, the range of step A-F is not shown as the blue dotted line due to the different experimental conditions compared with experiment II. The injection procedure in experiment II is step A (0–7.61 PV), step B (7.61–15.23 PV), step C (15.23–17.51 PV), step D (17.51–22.85 PV), step E (22.85–25.13 PV), and step F (25.13–30.47 PV).(For interpretation of the references to colour in this figure legend, the reader is referred to the web version of this article.)

solutions to further investigate the association between MWCNTs and soil colloids in the presence of different cation types. Fig. 5a shows a plot of the soil mass percentage of the different size fractions. Results indicate that the soil was composed of 2.38% WDCs (1.51% in the range of 0.45–2 μm and 0.87% less than 0.45 μm), 11.5% silt (2–20 μm), and 86.2% sand (20–2000 μm). This size fractionation is comparable to that obtained by (Kasel et al., 2013b), with small variations likely due to the use of different soil fractionation methods.

Fig. 5b presents a plot of the recovered mass percentages of MWCNTs in the various soil size fractions when the IS = 1 mM KCl and $CaCl_2$. The total mass recovery was calculated to be more than 85%. Mass percentages of MWCNTs in the sand and silt fractions were only 9.5 and 17.2%, respectively, even though they accounted for 97.7% of the soil mass. Mass percentage of MWCNTs in the 0.45–2 μm WDC fraction that accounted for 1.51% of the soil mass was 23.6%. The mass percentage of MWCNTs in the <0.45 μm WDC fraction and the so-called electrolyte phase (Jiang et al., 2014) was 49.7%. This fraction included MWCNTs associated with very fine soil colloids and those released during the fractionation procedure.

Fig. 5c presents the retained concentration (S/C_o) of MWCNTs in different soil fractions in the presence of KCl or $CaCl_2$ when the IS = 1 mM. The retained concentration of MWCNTs in each soil fraction was more pronounced in the presence of Ca^{2+} than K^+, especially in the WDC fraction. This observation can be explained by charge reversal/neutralization (Grosberg et al., 2002) and/or bridging complexation between soil grains and functionalized MWCNTs in the presence of Ca^{2+} (Torkzaban et al., 2012). Similar to experimental observations, bridging complexation is expected to be more pronounced with the WDC fraction (Torkzaban et al., 2012).

The above information indicates that the WDC fractions were enriched in MWCNTs in comparison with the sand and silt fractions, and that the association between WDCs and MWCNTs was related to the cation valance. This strong association between WDCs and MWCNTs provides further evidence for colloid-facilitated transport of MWCNTs during the release experiments.

4. Conclusions

Findings in this study provide important insight on the roles of solution IS, cation valance, and soil colloids on the transport, retention, and remobilization of MWCNTs in soils. Experimental and modeling results indicate that the mobility of MWCNTs was highly sensitivity to the IS and cation valence, with greater amounts of retention occurring at high IS and with divalent cations. BTCs for MWCNTs exhibited a delay in breakthrough that increased with solution IS and cation valence due to blocking. RPs for MWCNTs showed a hyper-exponential shape likely due to surface straining processes. Significant amounts of MWCNTs could be released by perturbations in solution chemistry that reduced the adhesive force (e.g., IS reduction and cation exchange). This release behavior was demonstrated to depend on the concentration of Ca^{2+} during MWCNT deposition and the release of soil colloids with a high

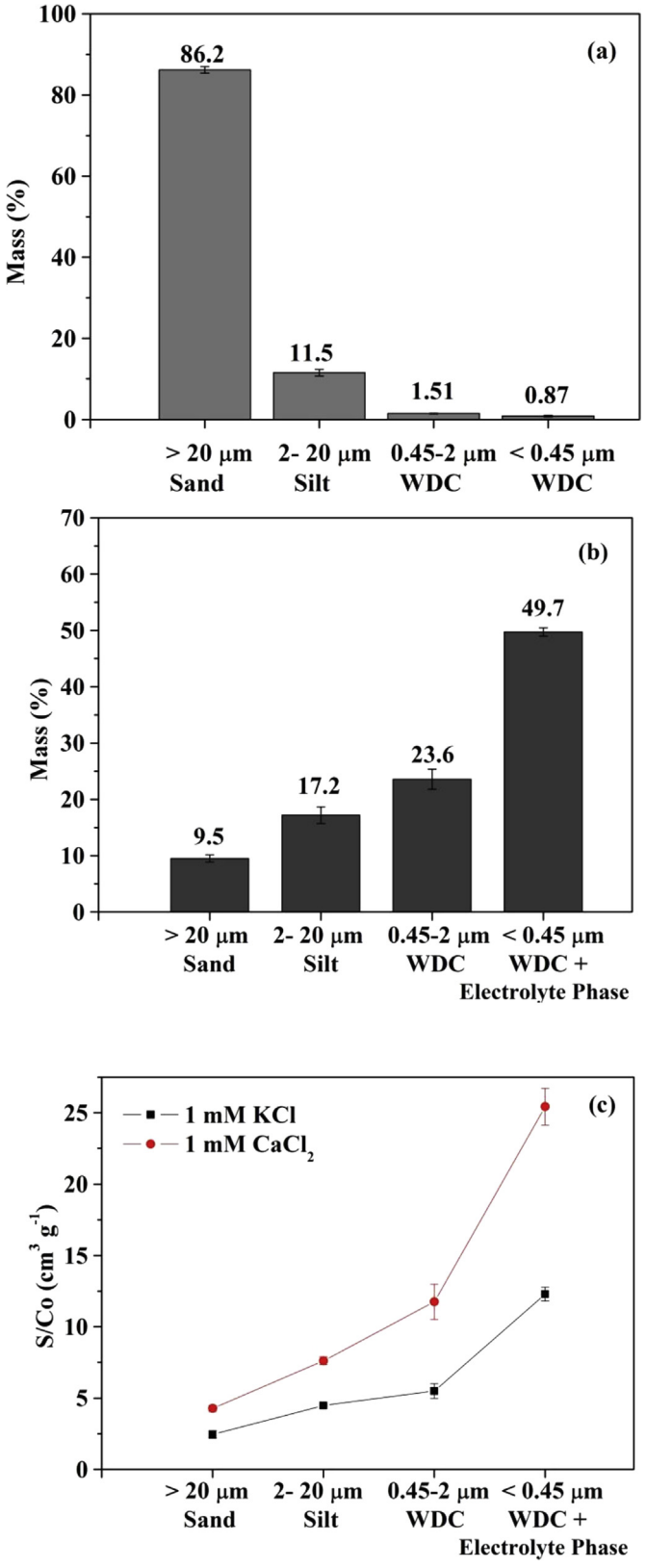

Fig. 5. (a) Mass percentage of each soil sized fraction: sand, silt, 0.45–2 μm WDCs and <0.45 μm WDCs; (b) Mass percentage of MWCNTs in sand, silt and 0.45–2 μm WDCs of soil. The <0.45 μm WDCs also contained the MWCNTs in the so-called electrolyte phase (1 mM KCl and $CaCl_2$); (c) Retained MWCNTs in sand, silt, 0.45–2 μm WDCs and <0.45 μm WDCs including electrolyte phase under different cation type.

association for MWCNTs. These results suggest the potential for soil colloids to facilitated the transport of MWCNTs in the subsurface environment, and thereby pose a potential risk of groundwater pollution, especially during rainfall or irrigation events that alter the solution chemistry.

Acknowledgments

The first author thanks the China Scholarship Council (CSC) for financial support. The authors would like to acknowledge Stephan Köppchen for bromide measurement, and Andrea Kubika and Martina Krause for TOC measurements. Thanks to Herbert Philipp and Claudia Walraf for their technical assistance, and Xiaoqian Jiang and Wulf Amelung for the helpful discussion related to soil fractionation.

References

Badawy, A.M.E., Luxton, T.P., Silva, R.G., Scheckel, K.G., Suidan, M.T., Tolaymat, T.M., 2010. Impact of environmental conditions (pH, ionic strength, and electrolyte type) on the surface charge and aggregation of silver nanoparticles suspensions. Environ. Sci. Technol. 44 (4), 1260–1266.
Bradford, S.A., Bettahar, M., 2006. Concentration dependent transport of colloids in saturated porous media. J. Contam. Hydrol. 82 (1), 99–117.
Bradford, S.A., Kim, H., 2010. Implications of cation exchange on clay release and colloid-facilitated transport in porous media. J. Environ. Qual. 39 (6), 2040.
Bradford, S.A., Kim, H.N., Haznedaroglu, B.Z., Torkzaban, S., Walker, S.L., 2009. Coupled factors influencing concentration-dependent colloid transport and retention in saturated porous media. Environ. Sci. Technol. 43 (18), 6996–7002.
Bradford, S.A., Šimůnek, J., Bettahar, M., van Genuchten, M.T., Yates, S.R., 2003. Modeling colloid attachment, straining, and exclusion in saturated porous media. Environ. Sci. Technol. 37 (10), 2242–2250.
Bradford, S.A., Torkzaban, S., 2008. Colloid transport and retention in unsaturated porous media: a review of interface-, collector-, and pore-scale processes and models. Vadose Zone J. 7 (2), 667–681.
Bradford, S.A., Torkzaban, S., 2013. Colloid interaction energies for physically and chemically heterogeneous porous media. Langmuir 29 (11), 3668–3676.
Bradford, S.A., Torkzaban, S., 2015. Determining parameters and mechanisms of colloid retention and release in porous media. Langmuir 31 (44), 12096–12105.
Bradford, S.A., Yates, S.R., Bettahar, M., Šimůnek, J., 2002. Physical factors affecting the transport and fate of colloids in saturated porous media. Water Resour. Res. 38 (12), 63-1–63-12.
Camilli, L., Pisani, C., Gautron, E., Scarselli, M., Castrucci, P., D'Orazio, F., Passacantando, M., Moscone, D., De Crescenzi, M., 2014. A three-dimensional carbon nanotube network for water treatment. Nanotechnology 25 (6), 065701.
Chen, K.L., Elimelech, M., 2006. Aggregation and deposition kinetics of fullerene (C_{60}. Nanoparticles. Langmuir 22 (26), 10994–11001.
Chen, K.L., Elimelech, M., 2007. Influence of humic acid on the aggregation kinetics of fullerene (C_{60}) nanoparticles in monovalent and divalent electrolyte solutions. J. Colloid Interface Sci. 309 (1), 126–134.
Cornelis, G., Hund-Rinke, K., Kuhlbusch, T., Van den Brink, N., Nickel, C., 2014. Fate and bioavailability of engineered nanoparticles in soils: a review. Crit. Rev. Environ. Sci. Technol. 44 (24), 2720–2764.
de Jonge, L.W., Moldrup, P., Rubæk, G.H., Schelde, K., Djurhuus, J., 2004. Particle leaching and particle-facilitated transport of phosphorus at field scale. Vadose Zone J. 3 (2), 462–470.
Elimelech, M., Gregory, J., Jia, X., 2013. Particle Deposition and Aggregation: Measurement, Modelling and Simulation. Butterworth-Heinemann.
Gao, B., Saiers, J.E., Ryan, J., 2006. Pore-scale mechanisms of colloid deposition and mobilization during steady and transient flow through unsaturated granular media. Water Resour. Res. 42 (1).
Gohardani, O., Elola, M.C., Elizetxea, C., 2014. Potential and prospective implementation of carbon nanotubes on next generation aircraft and space vehicles: a review of current and expected applications in aerospace sciences. Prog. Aerosp. Sci. 70, 42–68.
Grolimund, D., Borkovec, M., 2005. Colloid-facilitated transport of strongly sorbing contaminants in natural porous media: mathematical modeling and laboratory column experiments. Environ. Sci. Technol. 39 (17), 6378–6386.
Grolimund, D., Borkovec, M., 2006. Release of colloidal particles in natural porous media by monovalent and divalent cations. J. Contam. Hydrol. 87 (3), 155–175.
Grosberg, A.Y., Nguyen, T., Shklovskii, B., 2002. Colloquium: the physics of charge inversion in chemical and biological systems. Rev. Mod. Phys. 74 (2), 329.
Guldi, D.M., Rahman, G., Prato, M., Jux, N., Qin, S., Ford, W., 2005. Single-wall carbon nanotubes as integrative building blocks for solar-energy conversion. Angew. Chem. 117 (13), 2051–2054.
Hassellöv, M., Readman, J.W., Ranville, J.F., Tiede, K., 2008. Nanoparticle analysis and characterization methodologies in environmental risk assessment of engineered nanoparticles. Ecotoxicology 17 (5), 344–361.
Iijima, S., 1991. Helical microtubules of graphitic carbon. Nature 354 (6348), 56–58.

Israelachvili, J.N., 2011. Intermolecular and Surface Forces, revised third ed. Academic press.
Jaisi, D.P., Saleh, N.B., Blake, R.E., Elimelech, M., 2008. Transport of single-walled carbon nanotubes in porous media: filtration mechanisms and reversibility. Environ. Sci. Technol. 42 (22), 8317–8323.
Janas, D., Herman, A.P., Boncel, S., Koziol, K.K., 2014. Iodine monochloride as a powerful enhancer of electrical conductivity of carbon nanotube wires. Carbon 73, 225–233.
Jiang, C.-L., Séquaris, J.-M., Vereecken, H., Klumpp, E., 2012. Effects of inorganic and organic anions on the stability of illite and quartz soil colloids in Na-, Ca-and mixed Na–Ca systems. Colloids Surf. A Physicochem. Eng. Asp. 415, 134–141.
Jiang, C., Séquaris, J.-M., Wacha, A., Bóta, A., Vereecken, H., Klumpp, E., 2014. Effect of metal oxide on surface area and pore size of water-dispersible colloids from three German silt loam topsoils. Geoderma 235, 260–270.
Jones, A.D.K., Bekkedahl, T., 1997. Storage of hydrogen in single-walled carbon nanotubes. Nature 386, 377.
Kasel, D., Bradford, S.A., Šimůnek, J., Heggen, M., Vereecken, H., Klumpp, E., 2013a. Transport and retention of multi-walled carbon nanotubes in saturated porous media: effects of input concentration and grain size. Water Res. 47 (2), 933–944.
Kasel, D., Bradford, S.A., Šimůnek, J., Pütz, T., Vereecken, H., Klumpp, E., 2013b. Limited transport of functionalized multi-walled carbon nanotubes in two natural soils. Environ. Pollut. 180 (0), 152–158.
Khilar, K.C., Fogler, H.S., 1998. Migrations of Fines in Porous Media. Springer Science & Business Media.
Leij, F.J., Bradford, S.A., Wang, Y., Sciortino, A., 2015. Langmuirian blocking of irreversible colloid retention: analytical solution, moments, and setback distance. J. Environ. Qual. 44 (5), 1473–1482.
Li, C., Schäffer, A., Séquaris, J.-M., László, K., Tóth, A., Tombácz, E., Vereecken, H., Ji, R., Klumpp, E., 2012. Surface-associated metal catalyst enhances the sorption of perfluorooctanoic acid to multi-walled carbon nanotubes. J. Colloid Interface Sci. 377 (1), 342–346.
Li, X., Zhang, P., Lin, C., Johnson, W.P., 2005. Role of hydrodynamic drag on microsphere deposition and Re-Entrainment in porous media under unfavorable conditions. Environ. Sci. Technol. 39 (11), 4012–4020.
Liang, Y., Bradford, S.A., Šimůnek, J., Heggen, M., Vereecken, H., Klumpp, E., 2013. Retention and remobilization of stabilized silver nanoparticles in an undisturbed loamy sand soil. Environ. Sci. Technol. 47 (21), 12229–12237.
Lin, H., Zhu, H., Guo, H., Yu, L., 2008. Microwave-absorbing properties of Co-Filled carbon nanotubes. Mater. Res. Bull. 43 (10), 2697–2702.
Mauter, M.S., Elimelech, M., 2008. Environmental applications of carbon-based nanomaterials. Environ. Sci. Technol. 42 (16), 5843–5859.
McNew, C.P., LeBoeuf, E.J., 2016. Nc60 deposition kinetics: the complex contribution of humic acid, ion concentration, and valence. J. Colloid Interface Sci. 473, 132–140.
Pan, B., Xing, B., 2012. Applications and implications of manufactured nanoparticles in soils: a review. Eur. J. Soil Sci. 63 (4), 437–456.
Pauluhn, J., 2010. Multi-walled carbon nanotubes (Baytubes®): approach for derivation of occupational exposure limit. Regul. Toxicol. Pharmacol. 57 (1), 78–89.
Pecora, R., 2000. Dynamic light scattering measurement of nanometer particles in liquids. J. Nanoparticle Res. 2 (2), 123–131.
Sasidharan, S., Torkzaban, S., Bradford, S.A., Dillon, P.J., Cook, P.G., 2014. Coupled effects of hydrodynamic and solution chemistry on long-term nanoparticle transport and deposition in saturated porous media. Colloids Surf. A Physicochem. Eng. Asp. 457, 169–179.
Séquaris, J.-M., Lewandowski, H., 2003. Physicochemical characterization of potential colloids from agricultural topsoils. Colloids Surf. A Physicochem. Eng. Asp. 217 (1), 93–99.
Šimůnek, J., Genuchten, M.T.V., Šejna, M., 2016. Recent developments and applications of the hydrus computer software packages. Vadose Zone J. 15 (7), 25. http://dx.doi.org/10.2136/vzj2016.04.0033.
Tian, Y., Gao, B., Wu, L., Munoz-Carpena, R., Huang, Q., 2012. Effect of solution chemistry on multi-walled carbon nanotube deposition and mobilization in clean porous media. J. Hazard. Mater. 231–232, 79–87.
Tong, M., Johnson, W.P., 2007. Colloid population heterogeneity drives hyperexponential deviation from classic filtration theory. Environ. Sci. Technol. 41 (2), 493–499.
Torkzaban, S., Bradford, S.A., Wan, J., Tokunaga, T., Masoudih, A., 2013. Release of quantum dot nanoparticles in porous media: role of cation exchange and aging time. Environ. Sci. Technol. 47 (20), 11528–11536.
Torkzaban, S., Wan, J., Tokunaga, T.K., Bradford, S.A., 2012. Impacts of bridging complexation on the transport of surface-modified nanoparticles in saturated sand. J. Contam. Hydrol. 136, 86–95.
Tufenkji, N., Elimelech, M., 2005. Spatial distributions of cryptosporidium oocysts in porous media: evidence for dual mode deposition. Environ. Sci. Technol. 39 (10), 3620–3629.
Wang, D., Jaisi, D.P., Yan, J., Jin, Y., Zhou, D., 2015. Transport and retention of polyvinylpyrrolidone-coated silver nanoparticles in natural soils. Vadose Zone J. 14 (7).
Wang, Y., Bradford, S.A., Šimůnek, J., 2014. Physicochemical factors influencing the preferential transport of in soils. Vadose Zone J. 13 (1).
Wang, Y., Kim, J.H., Baek, J.B., Miller, G.W., Pennell, K.D., 2012. Transport behavior of functionalized multi-wall carbon nanotubes in water-saturated quartz sand as a function of tube length. Water Res. 46 (14), 4521–4531.
Yan, J., Lazouskaya, V., Jin, Y., 2016. Soil colloid release affected by dissolved organic matter and redox conditions. Vadose Zone J. 15 (3).
Yang, J., Bitter, J.L., Smith, B.A., Fairbrother, D.H., Ball, W.P., 2013. Transport of oxidized multi-walled carbon nanotubes through silica based porous media: influences of aquatic chemistry, surface chemistry, and natural organic matter. Environ. Sci. Technol. 47 (24), 14034–14043.
Zhang, S., Shao, T., Kose, H.S., Karanfil, T., 2010. Adsorption of aromatic compounds by carbonaceous adsorbents: a comparative study on granular activated carbon, activated carbon fiber, and carbon nanotubes. Environ. Sci. Technol. 44 (16), 6377–6383.
Zhang, M., Bradford, S.A., Simunek, J., Vereecken, H., Klumpp, E., 2016. Do goethite surfaces really control the transport and retention of multi-walled carbon nanotubes in chemically heterogeneous porous media? Environ. Sci. Technol. http://dx.doi.org/10.1021/acs.est.6b03285.
Zhu, Y., Ma, L.Q., Dong, X., Harris, W.G., Bonzongo, J., Han, F., 2014. Ionic strength reduction and flow interruption enhanced colloid-facilitated Hg transport in contaminated soils. J. Hazard. Mater. 264, 286–292.